Mean-field density-functional model of a second-order wetting transition

K. Koga[1,a)] and B. Widom[2]
[1]*Department of Chemistry, Faculty of Science, Okayama University, Okayama 700-8530, Japan*
[2]*Department of Chemistry, Baker Laboratory, Cornell University, Ithaca, New York 14853-1301, USA*

(Received 22 January 2008; accepted 19 February 2008; published online 21 March 2008)

First- and second-order wetting transitions are contrasted. A mean-field density-functional model that leads to a second-order transition is introduced. The way in which it differs from an earlier, otherwise similar model in which the transition is first order is noted. The interfacial and line tensions in the model are obtained numerically and their behavior on approach to the transition is determined. The spatial variation of the model's densities in the neighborhood of the contact line near the wetting transition is also found and seen to be characteristically different at a second-order transition from what it is at a first-order transition. The results for the line tension and for the spatial variation of the densities are in accord with those from an earlier interface-displacement model of the same phenomena. © *2008 American Institute of Physics*. [DOI: 10.1063/1.2895748]

I. INTRODUCTION

We consider three phases α, β, γ in equilibrium, with the interfacial tensions $\sigma_{\alpha\beta}, \sigma_{\beta\gamma}, \sigma_{\alpha\gamma}$. When $\sigma_{\alpha\gamma}=\sigma_{\alpha\beta}+\sigma_{\beta\gamma}$ ("Antonoff's rule"), the β phase intrudes at ("wets") the $\alpha\gamma$ interface and there is no direct $\alpha\gamma$ contact. When, instead, $\sigma_{\alpha\gamma}<\sigma_{\alpha\beta}+\sigma_{\beta\gamma}$ ("Neumann triangle"), the three phases meet at a line of common contact, associated with which is an excess free energy per unit length, the line tension[1] τ. With varying thermodynamic state there may be a transition between these two modes of three-phase equilibrium, termed a wetting transition.

In the Neumann-triangle regime the phases meet at their line of common contact with definite contact angles determined by the tensions. We denote these angles by α, β, γ, naming them for the phases through which they are measured. They are given in terms of the tensions by, for example,[2]

$$1-\cos\beta=\frac{\sigma_{\alpha\beta}+\sigma_{\beta\gamma}+\sigma_{\alpha\gamma}}{2\sigma_{\alpha\beta}\sigma_{\beta\gamma}}(\sigma_{\alpha\beta}+\sigma_{\beta\gamma}-\sigma_{\alpha\gamma}). \tag{1}$$

On approaching the transition from nonwetting to wetting of the $\alpha\gamma$ interface by the β phase, $\beta\to 0$ and $\sigma_{\alpha\gamma}\to\sigma_{\alpha\beta}+\sigma_{\beta\gamma}$, so β vanishes proportionally to the square root of $\sigma_{\alpha\beta}+\sigma_{\beta\gamma}-\sigma_{\alpha\gamma}$:

$$\beta\sim(\sigma_{\alpha\beta}+\sigma_{\beta\gamma}-\sigma_{\alpha\gamma})^{1/2}. \tag{2}$$

In the simplest cases, in mean-field theory, one distinguishes first- and second-order wetting transitions (although there can be more complex behavior, such as sequential wetting in which a partially frustrated first-order transition is followed by a higher-order wetting transition[3,4]). Figure 1 illustrates the distinction. A thermodynamic field variable (temperature or a chemical potential) there called b varies through the region of three-phase coexistence. The wetting transition occurs at $b=b_w$, with $b>b_w$ the regime in which the $\alpha\gamma$ interface is not wet by the β phase and $b<b_w$ that in which it is. The figure depicts the variation of $\sigma_{\alpha\beta}+\sigma_{\beta\gamma}-\sigma_{\alpha\gamma}$ with b. In Fig. 1(a) the wetting transition is first order: $\sigma_{\alpha\beta}+\sigma_{\beta\gamma}-\sigma_{\alpha\gamma}$ vanishes proportionally to the first power of $b-b_w$ and has a metastable extension, indicated by the dashed line, where the nonwet structure of the $\alpha\gamma$ interface may persist when the stable structure of that interface would be that in which it is wet by β. When $b<b_w$, both structures yield local free-energy minima, while that of the wet interface is the global minimum. Figure 1(b) depicts a second-order wetting transition: $\sigma_{\alpha\beta}+\sigma_{\beta\gamma}-\sigma_{\alpha\gamma}$ vanishes proportionally to $(b-b_w)^2$ and there is no metastable extension to $b<b_w$. From Eq. (2), the first- and second-order wetting transitions may also be distinguished by the rate at which the contact angle β vanishes as $b\to b_w$:

$$\beta\sim(b-b_w)^{1/2}\quad\text{(first order)}, \tag{3}$$

$$\beta\sim b-b_w\quad\text{(second order)}. \tag{4}$$

How intermolecular interactions of different strengths and ranges may lead to different orders of wetting transition has been much discussed in the literature (Refs. 5 and 6 and many references therein). In the next section we introduce a mean-field density-functional model of three-phase equilibrium that we later show to have a second-order wetting transition. The model is contrasted with a similar one that has been much studied in the past and is known to have a first-order wetting transition, thus showing that seemingly small differences in models can have not merely quantitative but also qualitative effects on the character of the transition.

The details of the numerical methods and analysis are in Sec. III and a brief summary is in Sec. IV.

II. MODEL

Our model free-energy functional Ψ, the density of excess free energy due to the density inhomogeneities at the interfaces and contact line, is a functional of two spatially varying densities $\rho_1(\mathbf{r})$ and $\rho_2(\mathbf{r})$ and a field variable b of the form

a)Electronic mail: koga@cc.okayama-u.ac.jp.

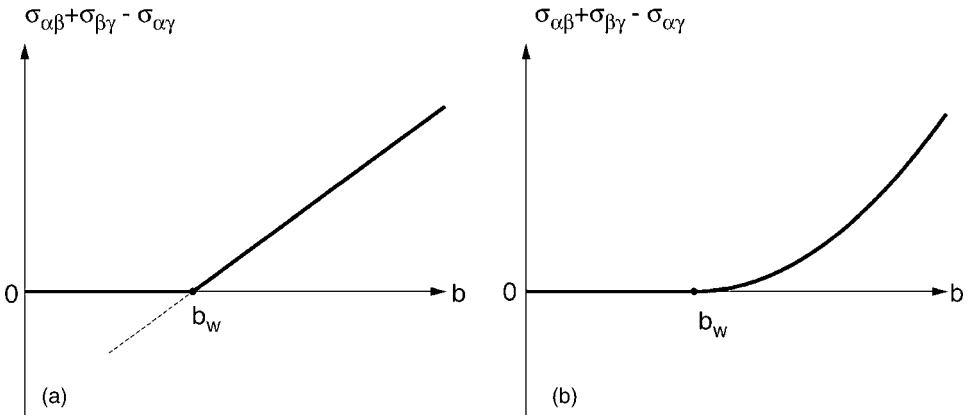

FIG. 1. (a) First-order wetting transition at $b=b_w$. (b) Second-order wetting transition at $b=b_w$.

$$\Psi = F[\rho_1(\mathbf{r}),\rho_2(\mathbf{r});b] + \tfrac{1}{2}(|\nabla\rho_1(\mathbf{r})|^2 + |\nabla\rho_2(\mathbf{r})|^2), \tag{5}$$

with

$$F(\rho_1,\rho_2;b) = [(\rho_1+1)^2+\rho_2^2][(\rho_1-1)^2+\rho_2^2] \times[\rho_1^2+(\rho_2-b)^2] \quad \text{(model B)}. \tag{6}$$

We call this model B to distinguish it from a much studied earlier model (Ref. 7 and many earlier papers), which we call model A. Instead of Eq. (6), which is a sixth-order polynomial in the densities, in model A one has the fourth-order polynomial

$$F(\rho_1,\rho_2;b) = 16\rho_2^2(\rho_2-b)^2 + [(\rho_2-b\rho_1)^2-b^2]^2 + [(\rho_2+b\rho_1)^2-b^2]^2 \quad \text{(model A)}. \tag{7}$$

In both models, for each b there are three phases α,β,γ in equilibrium, in which the densities, far from the interfaces and contact line, have the uniform values

$$\rho_1=-1,\ \rho_2=0 \ (\text{phase } \alpha); \qquad \rho_1=0,\ \rho_2=b \ (\text{phase } \beta);\ \rho_1=1,\ \rho_2=0 \ (\text{phase } \gamma). \tag{8}$$

At each of these bulk-phase compositions, in each model, F and both $\partial F/\partial\rho_1$ and $\partial F/\partial\rho_2$ vanish while $F>0$ at any other composition ρ_1,ρ_2. In spite of the seemingly great similarity of the two models, model A is known to have a first-order wetting transition in which the β phase wets the $\alpha\gamma$ interface, while in model B the transition is second order, as we shall show in Sec. III. The distinction is that between Figs. 1(a) and 1(b).

In the interfaces far from the contact line, the densities $\rho_1(\mathbf{r})$ and $\rho_2(\mathbf{r})$ vary only in the directions perpendicular to the interfaces. If for each interface separately a coordinate z is associated with the perpendicular direction, then the densities, as they vary through the interface, are functions $\rho_1(z),\rho_2(z)$ of z alone. The several interfacial tensions are variational integrals over z of the functional Ψ, minimized with respect to the $\rho_1(z),\rho_2(z)$ that satisfy Eqs. (8) at $z=\pm\infty$:

$$\sigma = \min_{\rho_1(z),\rho_2(z)} \int_{-\infty}^{\infty} \Psi dz, \tag{9}$$

where σ is in turn $\sigma_{\alpha\beta}$, $\sigma_{\beta\gamma}$, or $\sigma_{\alpha\gamma}$, according to which of the boundary conditions (8) the $\rho_1(z)$ and $\rho_2(z)$ are required to satisfy. The minimizing $\rho_1(z)$ and $\rho_2(z)$ give the equilibrium (or metastable) spatially varying composition of the interface. The variational minimum is achieved by the solution $\rho_1(z)$, $\rho_2(z)$ of the coupled Euler–Lagrange equations

$$\frac{\partial F}{\partial\rho_1} = \frac{d^2\rho_1}{dz^2}, \qquad \frac{\partial F}{\partial\rho_2} = \frac{d^2\rho_2}{dz^2} \tag{10}$$

subject to the same boundary conditions (8) for each interface in turn.

On eliminating z between $\rho_1(z)$ and $\rho_2(z)$ one has a trajectory in the ρ_1,ρ_2 plane, from one bulk-phase point ρ_1,ρ_2 of Eqs. (8) to another, showing how these densities vary with

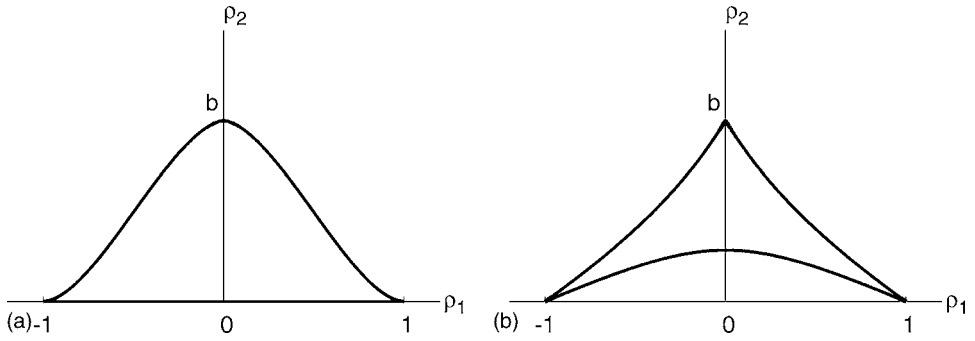

FIG. 2. (a) Model A. The horizontal line $\rho_2=0$ from $\rho_1=-1$ (α phase) to $\rho_1=+1$ (γ phase) gives the equilibrium (or metastable) structure of the $\alpha\gamma$ interface, while the curves from $\rho_1=-1$, $\rho_2=0$ (α phase) to $\rho_1=0$, $\rho_2=b$ (β phase) and from $\rho_1=+1$, $\rho_2=0$ (γ phase) to $\rho_1=0$, $\rho_2=b$ (β phase) give the structures of the $\alpha\beta$ and $\beta\gamma$ interfaces, respectively. (b) Model B. The curve from $\rho_1=-1$, $\rho_2=0$ (α phase) to $\rho_1=+1$, $\rho_2=0$ (γ phase) that does not pass through $\rho_1=0$, $\rho_2=b$ (β phase) gives the structure of the $\alpha\gamma$ interface, while the other two curves give the structures of the $\alpha\beta$ and $\beta\gamma$ interfaces.

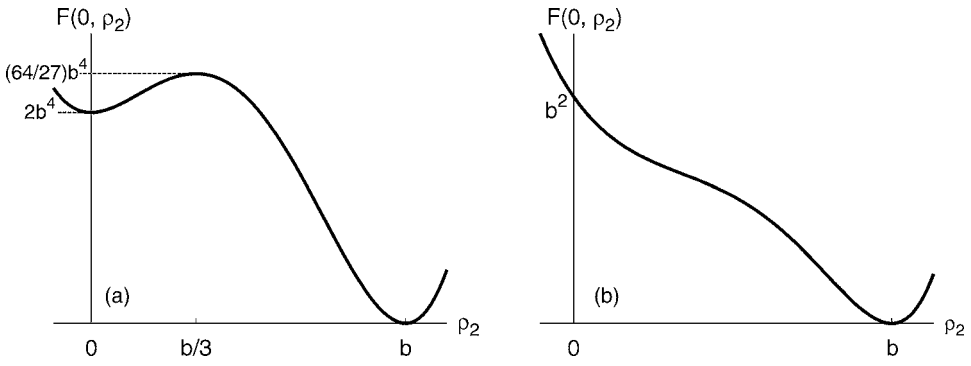

FIG. 3. $F(0,\rho_2;b)$ vs ρ_2 for fixed b. (a) Model A. (b) Model B for $b<\sqrt{3}$.

each other in the corresponding equilibrium (or metastable) interface far from the contact line. Such trajectories are shown in Figs. 2(a) and 2(b), where Fig. 2(a) is characteristic of the earlier model A and Fig. 2(b) of the present model B. In model A [Fig. 2(a)] there is always a locally stable $\alpha\gamma$ interface in which (with an appropriate choice of the origin and direction of z)

$$\rho_2(z) \equiv 0, \quad \rho_1(z) = -\tanh(2b^2 z). \tag{11}$$

In model B there is no solution for the $\alpha\gamma$ interface in which $\rho_2(z)\equiv 0$; instead, there is a solution in which ρ_2 increases from 0 in the interior of the bulk α phase, reaches a maximum at which $\rho_1=0$, and then decreases to 0 again in the interior of the bulk γ phase.

When the free energy (the tension $\sigma_{\alpha\gamma}$) of the $\alpha\gamma$ interface associated with the trajectory in Fig. 2 that goes directly from α to γ, not via β, is less than that on the composite trajectory from α to β and β to γ, the stable structure of the $\alpha\gamma$ interface is that given by the direct trajectory, and the $\alpha\gamma$ interface is not wet by the β phase. When the composite trajectory via β is that of the lower tension, the stable $\alpha\gamma$ interface is that which is wet by β, and consists of a macroscopically thick layer of β bounded by normal $\alpha\beta$ and $\beta\gamma$ interfaces, with $\sigma_{\alpha\gamma}$ then equal to $\sigma_{\alpha\beta}+\sigma_{\beta\gamma}$. In model A, the transition between these two alternative structures of the $\alpha\gamma$ interface occurs while the indirect (via β) and direct trajectories from α to γ in Fig. 2(a) are still distinct. That is a first-order transition in the structure of the $\alpha\gamma$ interface. In model B, by contrast, $\sigma_{\alpha\gamma}$ comes to approach and then equal $\sigma_{\alpha\beta}+\sigma_{\beta\gamma}$ only when the direct $\alpha\gamma$ trajectory in Fig. 2(b) comes to approach and then coincide with the indirect trajectory via β. That is a second-order wetting transition. At the first-order transition there is thus a discontinuity in the structure of the $\alpha\gamma$ interface with an associated discontinuity in $d\sigma_{\alpha\gamma}/db$, and so also in $d(\sigma_{\alpha\beta}+\sigma_{\beta\gamma}-\sigma_{\alpha\gamma})/db$ [Fig. 1(a)], since $d\sigma_{\alpha\beta}/db$ and $d\sigma_{\beta\gamma}/db$ are continuous; while at the second-order transition, the structure of the $\alpha\gamma$ interface is continuous and so too are $d\sigma_{\alpha\gamma}/db$ and $d(\sigma_{\alpha\beta}+\sigma_{\beta\gamma}-\sigma_{\alpha\gamma})/db$ (=0).

The differences between the $F(\rho_1,\rho_2;b)$ of models A and B are subtle, but one difference that may be implicated in the one having a first-order and the other a second-order wetting transition is shown in Fig. 3, where $F(0,\rho_2;b)$ is sketched as a function of ρ_2 for fixed b. This shows how the local free-energy density F varies with ρ_2 as a representative point at $\rho_1=0$ in Figs. 2(a) and 2(b) moves vertically upward from $\rho_2=0$ to the β phase at $\rho_2=b$. In Fig. 3(a), for model A, one sees a maximum at $\rho_2=b/3$, implying a potential hill at $\rho_1=0,\rho_2=b/3$ in the plane of Fig. 2(a). This could have blocked the direct $\alpha\gamma$ trajectory from passing through $\rho_2=b/3$, and thus blocked it from ultimately coinciding with the indirect trajectory via β at a second-order transition (even if, as in model A, the direct trajectory had not anyway been confined to the $\rho_2=0$ axis). In model B, by contrast, for any $b\leqslant\sqrt{3}$, there is no such free-energy barrier, so nothing to block the direct $\alpha\gamma$ trajectory from passing through any value of ρ_2, ultimately coinciding with the indirect trajectory.

The first- and second-order wetting transitions are also distinguished by characteristically different shapes of the contours of constant $\rho_1(\mathbf{r})$ and $\rho_2(\mathbf{r})$ at the three-phase contact line, as the transition is being approached. Thus, the spatial structure of the contact line itself is different at a first-order wetting transition from what it is at a second-order transition. These contours are displayed in Sec. III.

The densities $\rho_1(\mathbf{r})$ and $\rho_2(\mathbf{r})$ are uniform in the direction of the contact line but vary in any plane perpendicular to that line. In both models A and B the line tension τ is obtained by minimizing with respect to $\rho_1(\mathbf{r})$ and $\rho_2(\mathbf{r})$ the integral of the excess free-energy density Ψ over a large (ultimately infinite, in principle) area in any such plane. The minimum is achieved when $\rho_1(\mathbf{r})$ and $\rho_2(\mathbf{r})$ satisfy the coupled Euler–Lagrange equations [analogous to (10) for the interfaces far from the contact line]

$$\frac{\partial F}{\partial \rho_1} = \nabla^2 \rho_1, \quad \frac{\partial F}{\partial \rho_2} = \nabla^2 \rho_2, \tag{12}$$

where ∇^2 is the two-dimensional Laplacian. These are to be solved subject to the conditions that $\rho_1(\mathbf{r})$ and $\rho_2(\mathbf{r})$ reduce to Eqs. (8) in the bulk phases, far from the interfaces and contact line, and reduce to the $\rho_1(z)$ and $\rho_2(z)$ for each interface far from the contact line, as determined from the solutions of Eqs. (10). Once the equilibrium $\rho_1(\mathbf{r})$ and $\rho_2(\mathbf{r})$ are determined in this way, the line tension τ may then be found from the Kerins–Boiteux integral,[8]

$$\tau = \int (\Psi - 2F) da, \tag{13}$$

where the integration is over the whole plane perpendicular to the contact line (the integrand being short ranged), with da the element of the area. This was earlier done[7] for model A and is now done for model B in Sec. III.

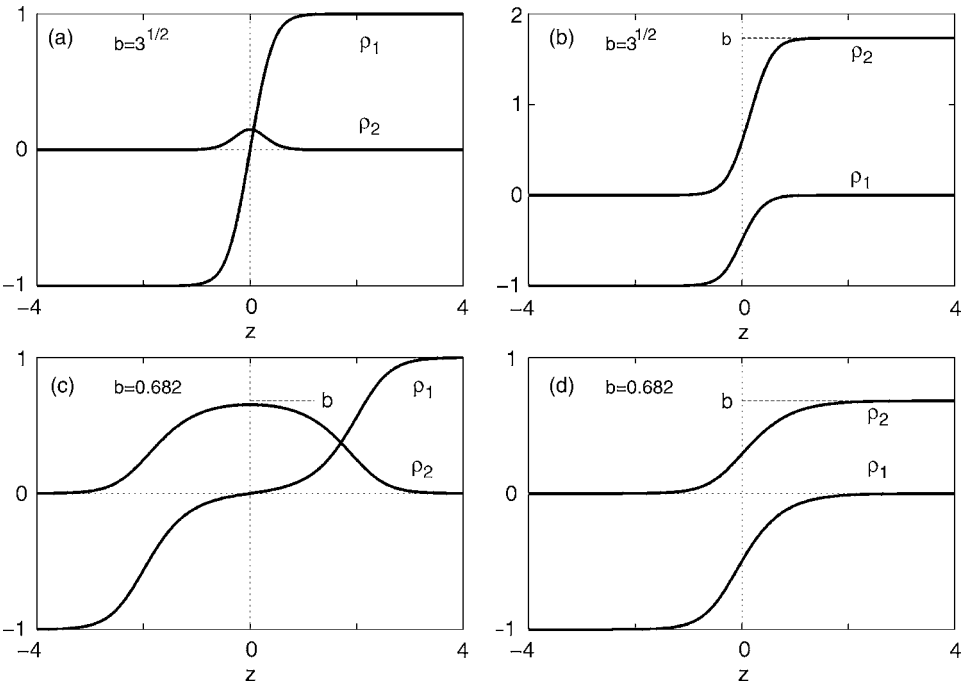

FIG. 4. Density profiles $\rho_1(z)$, $\rho_2(z)$. (a) $\alpha\gamma$ interface, $b=\sqrt{3}$. (b) $\alpha\beta$ interface, $b=\sqrt{3}$. (c) $\alpha\gamma$ interface, $b=0.682$. (d) $\alpha\beta$ interface, $b=0.682$.

Indekeu[9,10] had shown from an interface-displacement model that in mean-field approximation with short-range forces, as $b\to b_w$ at a first-order wetting transition, τ approaches its finite limiting value τ_w as

$$\tau \sim \tau_w - c\sqrt{b-b_w}\,\ln[1/(b-b_w)] \tag{14}$$

with some constant c. This behavior was verified numerically for model A in Ref. 7, with $c\simeq 0.455$. Indekeu[9,10] has also shown from his interface-displacement model that with short-range forces in mean-field approximation, on approach to a second-order wetting transition, τ vanishes through a range of negative values proportionally to the first power of the contact angle β, or, from Eq. (4),

$$\tau \sim -k(b-b_w), \tag{15}$$

with a positive coefficient of proportionality k. We shall verify Eq. (15) and the corresponding behavior with β, for model B, in Sec. III.

III. NUMERICAL METHODS AND RESULTS

The density profiles $\rho_1(z)$ and $\rho_2(z)$ of interfaces that minimize $\int\Psi dz$ are obtained by numerically solving the coupled Euler–Lagrange Eqs. (10) subject to the boundary conditions (8). As in the earlier study of model A,[7] the Euler–Lagrange equations are approximated by five-point difference equations, and then solved iteratively with a successive overrelaxation (SOR) method.[11] The range of z is taken to be $[-10,10]$ and the minimizing $\rho_1(z)$ and $\rho_2(z)$ are calculated on a uniform grid with spacing $h=0.005$. The initial guesses of $\rho_1(z)$ and $\rho_2(z)$ are taken to be step functions with two intervals separated at $z=0$. For the $\alpha\gamma$ interface near the wetting transition, the initial $\rho_1(z)$ and $\rho_2(z)$ are chosen to be step functions with three intervals separated at $z=\pm z_\beta$ with an appropriate z_β. The criterion for convergence is an rms difference of less than 1×10^{-13} between iterates.

Figure 4 shows the density profiles $\rho_1(z)$ and $\rho_2(z)$ of the $\alpha\gamma$ and $\alpha\beta$ interfaces for two representative thermodynamic states, one far from the wetting transition ($b=\sqrt{3}$) and one very close to the transition ($b=0.682$).

Comparisons between Figs. 4(a) and 4(c) and between Figs. 4(b) and 4(d) show that as the wetting transition is approached the interfaces become less sharp and a β-like layer grows in the $\alpha\gamma$ interface. The $\alpha\gamma$ interface is symmetric by symmetry of model B (as it is also for model A): $\rho_1(z)$ and $\rho_2(z)$ are antisymmetric and symmetric, respectively, with respect to the z at which $\rho_1(z)=0$ [$z=0$ in Figs. 4(a) and 4(c)]. However, the $\alpha\beta$ and $\beta\gamma$ interfaces are not symmetric, as seen in Figs. 4(b) and 4(d), and they cannot be so, as shown below.

The densities $\rho_1(z)$ and $\rho_2(z)$ are characterized by exponential decay to their bulk-phase values with decay lengths ξ_1 and ξ_2. From the Euler–Lagrange equations one finds that

$$\xi_1=\xi_2=\frac{1}{2\sqrt{2(b^2+1)}} \tag{16}$$

for decay into the α and γ phases and

$$\xi_1=\xi_2=\frac{1}{\sqrt{2}(b^2+1)} \tag{17}$$

for decay into the β phase. From Eqs. (16) and (17), the $\alpha\beta$ and $\beta\gamma$ interfaces cannot be symmetric.

The interfacial tensions are obtained from numerical integration

$$\sigma=2\int F dz, \tag{18}$$

which is equivalent to Eq. (9) with the identity $\Psi=2F$ that holds for equilibrium $\rho_1(z)$ and $\rho_2(z)$. We find that numerical values of $\sigma^2_{\alpha\gamma}$ for several rational numbers of b^2 are very close to rational numbers. For example, $\sigma^2_{\alpha\gamma}=10.666\,666\,64\cdots\simeq 96/9$ for $b^2=3$, $\sigma^2_{\alpha\gamma}=3.555\,555\,554\cdots$

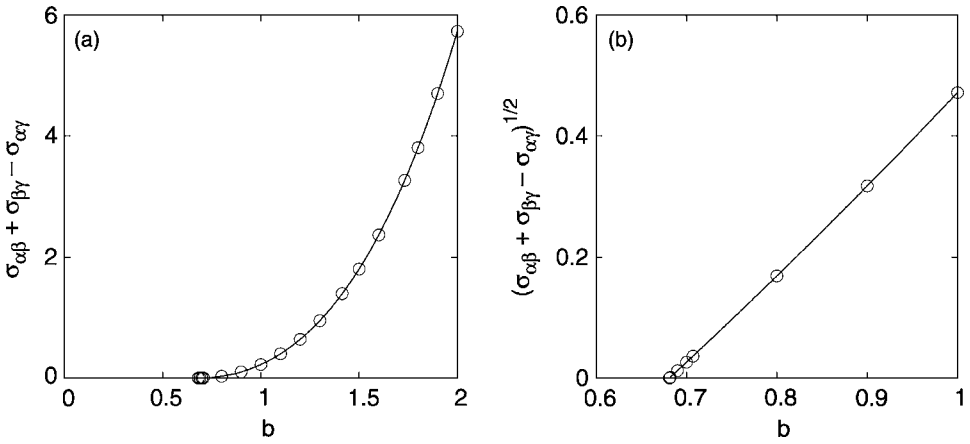

FIG. 5. (a) $\sigma_{\alpha\beta}+\sigma_{\beta\gamma}-\sigma_{\alpha\gamma}$ vs b. (b) $\sqrt{\sigma_{\alpha\beta}+\sigma_{\beta\gamma}-\sigma_{\alpha\gamma}}$ vs b. The points are numerical results and solid curves are those given by conjectured relations (19) and (20).

$\simeq 32/9$ for $b^2=1$, $\sigma^2_{\alpha\gamma}=1.777\,777\,777\cdots\simeq 16/9$ for $b^2=1/2$, etc. This implies the analytical formula $\sigma^2_{\alpha\gamma}=32b^2/9$ or

$$\sigma_{\alpha\gamma}=\frac{4\sqrt{2}}{3}b. \tag{19}$$

Conversely, it is checked that the above relation (19) holds for arbitrarily chosen b within numerical uncertainty in $\sigma_{\alpha\gamma}$. For the $\alpha\beta$ interface we find that $\sigma^2_{\alpha\beta}=0.125\,000\,000\cdots\simeq 1/8$ for $b^2=0$, $\sigma^2_{\alpha\beta}=0.445\,312\,500\cdots\simeq 57/128$ for $b^2=1/2$, $\sigma^2_{\alpha\beta}=1.111\,111\,111\cdots\simeq 10/9$ for $b^2=1$, $\sigma^2_{\alpha\beta}=4.124\,999\,995\cdots\simeq 33/8$ for $b^2=2$, and $\sigma^2_{\alpha\beta}=10.666\,666\,64\cdots\simeq 32/3$ for $b^2=3$. These results, too, imply an analytical form for $\sigma_{\alpha\beta}(b)$. If $\sigma^2_{\alpha\beta}$ is assumed to be a quartic polynomial in b^2 and the above rational numbers for $\sigma^2_{\alpha\beta}$ are taken to be exact, all the coefficients of the assumed polynomial are given by rational numbers:

$$\sigma^2_{\alpha\beta}=\tfrac{1}{8}+\tfrac{7}{18}b^2+\tfrac{5}{12}b^4+\tfrac{1}{6}b^6+\tfrac{1}{72}b^8. \tag{20}$$

For any other values of b examined, we find that the relative difference between Eq. (20) and the integral (18) is less than 10^{-8}.

In Fig. 5 are plotted $\sigma_{\alpha\beta}+\sigma_{\beta\gamma}-\sigma_{\alpha\gamma}$ and $(\sigma_{\alpha\beta}+\sigma_{\beta\gamma}-\sigma_{\alpha\gamma})^{1/2}$ as functions of b. The behavior in Fig. 5(a) is the same as that in Fig. 1(b); that is, in model B the wetting transition is second order. The linear fit of the two data points closest to wetting in Fig. 5(b) gives the numerical estimate: $b_w=0.681\,25\cdots$. The $\sigma_{\alpha\beta}+\sigma_{\beta\gamma}-\sigma_{\alpha\gamma}$ given by the conjectures (19) and (20) completely overlap with the numerical data points. Provided that Eqs. (19) and (20) are exact, the wetting transition is exactly determined as a solution of a quartic equation $(\sigma_{\alpha\beta}+\sigma_{\beta\gamma}-\sigma_{\alpha\gamma})(\sigma_{\alpha\beta}+\sigma_{\beta\gamma}+\sigma_{\alpha\gamma})=4\sigma^2_{\alpha\beta}-\sigma^2_{\alpha\gamma}=0$ for b^2 (note in the present model $\sigma_{\alpha\beta}=\sigma_{\beta\gamma}$). The solution is again given analytically:

$$b_w=\sqrt{2\sqrt{3}-3}=0.681\,250\,038\,633\cdots, \tag{21}$$

which is in agreement with the numerical estimate up to five digits. Indekeu[12] notes that this is also the solution to $(1+b)^{3/2}-(1-b)^{3/2}=2$, an equation he[13] ascribes to Cahn[14] and to Nakanishi and Fisher[15] in a related context. With the virtually perfect agreements with all the numerical results, we shall assume Eqs. (19)–(21) to be exact.

Trajectories in the ρ_1,ρ_2 plane, too, have what seem to be simple analytic expressions. Let θ_α, θ_β, and θ_γ be the asymptotic angles between trajectories at the bulk-phase points α, β, and γ in Fig. 2(b). In the fully symmetric case ($b=\sqrt{3}$), where $\theta_\alpha=\theta_\beta=\theta_\gamma$, the numerical calculation suggests the common value to be exactly 30°, so $\theta_\alpha+\theta_\beta+\theta_\gamma=90°$. At the second-order wetting ($b=b_w$), the direct $\alpha\gamma$ trajectory coincides with the indirect trajectory via β so that $\theta_\alpha=\theta_\gamma=0$. Numerical evaluation at the wetting transition suggests $\theta_\beta=90°$ (exactly). Thus, again, $\theta_\alpha+\theta_\beta+\theta_\gamma=90°$. In fact, numerical calculations for several values of b imply that

$$\theta_\alpha+\theta_\beta+\theta_\gamma=90° \tag{22}$$

for any b. Now let ϕ_α be the angle made by the direct $\alpha\gamma$ trajectory with the ρ_1 axis at α, and let A_β be the β vertex angle in the triangle $\alpha\beta\gamma$, where α,β,γ here stand for the bulk-phase points in the ρ_1,ρ_2 plane. Then numerical calculations suggest $4\phi_\alpha=A_\beta$ for any b. Since $\tan A_\beta/2=1/b$, this gives another relation,

$$\tan\phi_\alpha=-b+\sqrt{b^2+1}. \tag{23}$$

The angles $\theta_\beta/2$ and ϕ_α are related to the ratio of the amplitudes of exponential decays of the interfacial profiles to their bulk values. Let $\beta_{1,\alpha}$ and $\beta_{2,\alpha}$ be the amplitudes of asymptotic decay of ρ_1 and ρ_2 in the $\alpha\beta$ interface to their bulk β-phase values, and likewise let $\alpha_{1,\gamma}$ and $\alpha_{2,\gamma}$ be the amplitudes of the decay of ρ_1 and ρ_2 in the $\alpha\gamma$ interface to their values in the α phase. Then

$$\tan\frac{\theta_\beta}{2}=\frac{\beta_{1,\alpha}}{\beta_{2,\alpha}},\quad \tan\phi_\alpha=\frac{\alpha_{2,\gamma}}{\alpha_{1,\gamma}}. \tag{24}$$

The conjecture $\theta_\beta=90°$ at $b=b_w$ means that the amplitudes of the exponential decays of $\rho_1(z)$ and $\rho_2(z)$ to their bulk β-phase values become identical at the wetting transition: $\beta_{1,\alpha}=\beta_{2,\alpha}$, which we have verified numerically. Also, from Eq. (23), $\alpha_{2,\gamma}/\alpha_{1,\gamma}=-b+\sqrt{b^2+1}$. To check this, the amplitudes were evaluated from $\rho_1(z)$ and $\rho_2(z)$, and the relative deviation of $\alpha_{2,\gamma}/\alpha_{1,\gamma}$ from $-b+\sqrt{b^2+1}$ for several values of b was found to be less than 10^{-5}.

As described in Sec. II, the equilibrium $\rho_1(\mathbf{r})$ and $\rho_2(\mathbf{r})$ of three phases in contact are obtained as the solutions of

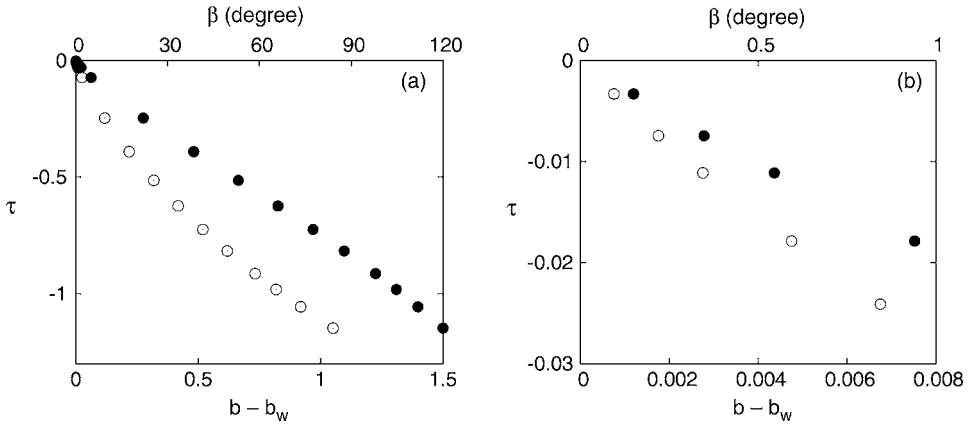

FIG. 6. τ vs b (○, bottom axis) and vs β (●, top axis) on a large scale (a) and near the wetting transition (b).

the Euler–Lagrange Eqs. (12). The coupled equations are discretized with a nine-point stencil and solved by the SOR method[11] for square-grid points with grid spacings d_x, d_y in an $L_x \times L_y$ rectangle, the x-axis being set parallel to the $\alpha\gamma$ interface. From the $\rho_1(\mathbf{r})$ and $\rho_2(\mathbf{r})$ thus obtained, the line tension τ is given by Eq. (13). The dimensions L_x, L_y of the rectangle must be sufficiently large for the inhomogeneity due to the three-phase contact to be absent on the sides of the rectangle; such L_x goes to infinity as b approaches b_w because the region affected by the three-phase contact extends indefinitely in the direction of the $\alpha\gamma$ interface as the contact angle β goes to 0. This is the main reason that numerical calculation of the line tension becomes a formidable task on approaching the wetting transition. To reduce the difficulty and to approach wetting as closely as possible we increase the grid spacing d_x with increasing L_x as b goes to b_w. It was checked that τ thus obtained is independent of d_x. This method is more effective for model B than for model A because in model B, with a scaled coordinate $x^* = x \tan(\beta/2)$ for the direction of the $\alpha\gamma$ interface, the variation in that direction is roughly independent of β near the second-order wetting transition. The closest to the wetting transition for which τ is obtained is $b=0.682$ and $\beta = 0.148\,79\cdots$ (in degrees), where $(L_x, L_y) = (20\,000, 20)$ and $(d_x, d_y) = (20, 0.02)$: Then the calculation completes in a few weeks with an eight-core 3.0 GHz Intel Xeon processor. The criterion for convergence is an rms difference in ρ_1 and ρ_2 of less than 1×10^{-11}.

The line tension τ is plotted against the field variable b and the contact angle β in Fig. 6. It is seen that τ is negative in the entire range of states and goes monotonically to zero as the wetting transition is approached. The slope $d\tau/db$ is *not* diverging in the same limit [Fig. 6(b)]. These results verify the asymptotic behavior (15) of τ given by Indekeu. The negative coefficient of proportionality $-k$ in Eq. (15) is found to be -4.57 ± 0.10 and the corresponding coefficient for the contact angle β to be -1.32 ± 0.06 rad^{-1}. The sum of the two ξ in Eqs. (16) and (17), evaluated at $b = b_w$, is around 0.8 and is a rough measure of the sum $\xi_{\alpha\beta} + \xi_{\beta\gamma}$ of the thicknesses of the $\alpha\beta$ and $\beta\gamma$ interfaces at wetting, while $\sigma_{\alpha\gamma}$, from Eq. (19), is 1.28. Thus, the product $(\xi_{\alpha\beta} + \xi_{\beta\gamma})\sigma_{\alpha\gamma} \approx 1$. Therefore, the -1.32 found here for the coefficient of the angle β on approach to wetting is close to $-(\xi_{\alpha\beta} + \xi_{\beta\gamma})\sigma_{\alpha\gamma}$. This, as remarked by Indekeu,[12] is as in the interface-displacement model.[9]

The spatial variations of ρ_1 and ρ_2 in model B in the neighborhood of the contact line near the second-order wetting transition and in model A near the first-order wetting transition are displayed as contour plots in Fig. 7. The distinction between the two cases is apparent: The contours of constant ρ_1 in model B are gently curved in the three-phase contact region whereas those of model A have a forklike shape. More precisely, for model B the slope of a contour varies monotonically from 0 to $\tan(\beta/2)$ or $-\tan(\beta/2)$ as x increases whereas for model A the magnitude of the slope varies from 0 to a value that exceeds $\tan(\beta/2)$ and then approaches the limiting value from above; i.e., the contours have inflection points. These are in accord with the analogous pictures found in the interface-displacement model of Indekeu (Figs. 1 and 7 of Ref. 9 or Figs. 10 and 14 of Ref. 10) and of Dobbs and Indekeu[16] (Figs. 4 and 5). (The ρ_2 contours in Figs. 7(c) and 7(d) mirror the ρ_1 contours in (a) and (b), except that the "handle" of the "fork" is missing in (c) because in model A, in the $\alpha\gamma$ interface far from the contact line, ρ_2 is identically 0 [Fig. 2(a)].) This further agreement between the density-functional and interface-displacement models is gratifying.

IV. SUMMARY

We consider three coexisting phases α, β, γ with $\sigma_{\alpha\beta}, \sigma_{\beta\gamma}, \sigma_{\alpha\gamma}$ the three interfacial tensions. The wetting transition between states in which the β phase does and does not wet the $\alpha\gamma$ interface is associated with the transition between the two conditions $\sigma_{\alpha\gamma} = \sigma_{\alpha\beta} + \sigma_{\beta\gamma}$ and $\sigma_{\alpha\gamma} < \sigma_{\alpha\beta} + \sigma_{\beta\gamma}$, respectively. The transition may be of first or second order. With b a thermodynamic control parameter (a field variable such as a chemical potential or the temperature) and b_w its value at the wetting transition, the first- and second-order transitions are characterized by Figs. 1(a) and 1(b), respectively. They are distinguished likewise by Eqs. (3) and (4), where β is the contact angle measured through the β phase as the wetting transition is approached from the nonwetting side ($b > b_w$).

An earlier mean-field density-functional model (here called model A) with a first-order wetting transition is recalled and a new model (model B) is introduced and later

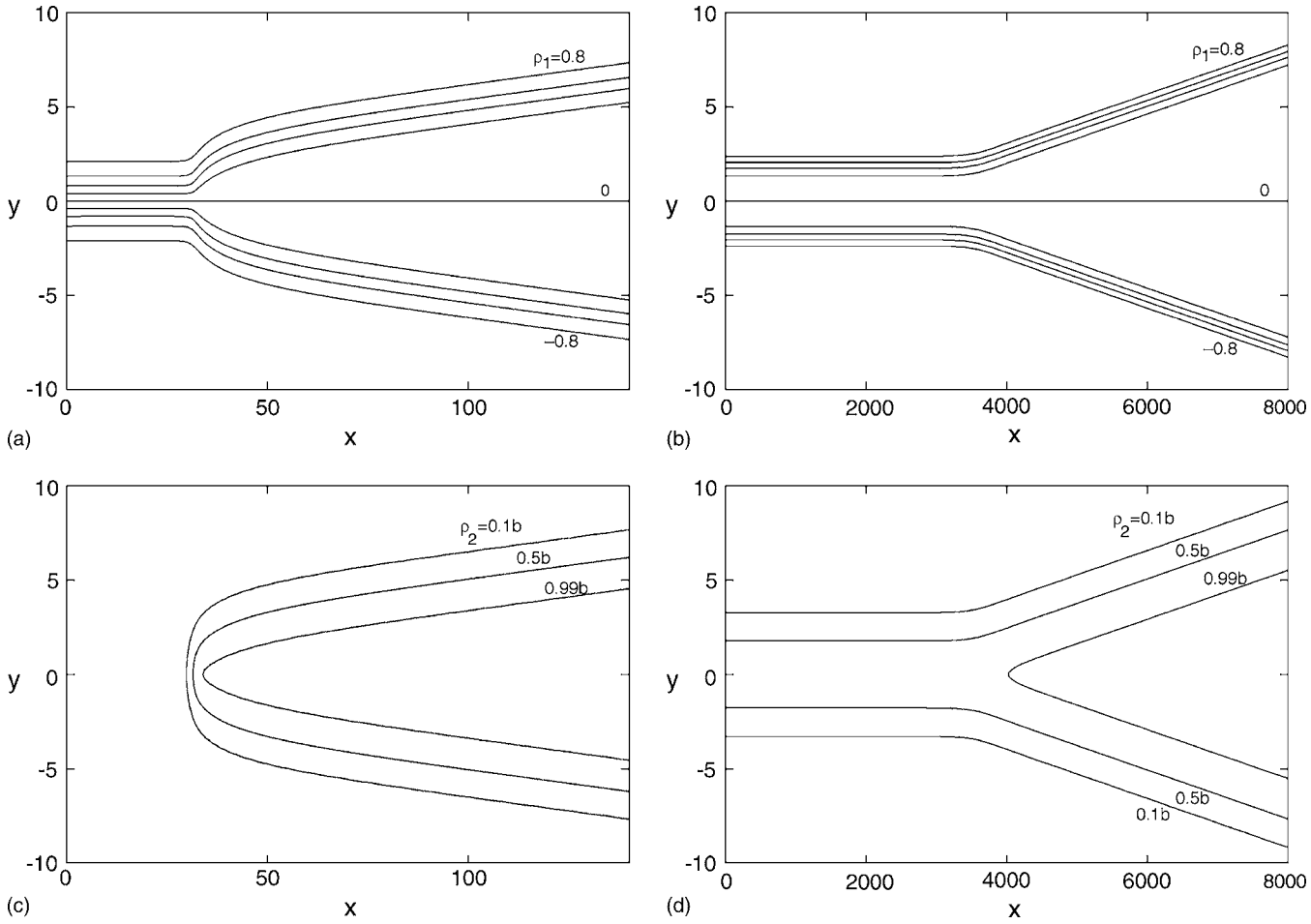

FIG. 7. Spatial variations of ρ_1 and ρ_2 in the neighborhood of the contact line near the wetting transition: (a) Contour plots of constant ρ_1 for model A (b=0.512, ρ_1=−0.8,…,0.8); (b) plots of constant ρ_1 for model B (b=0.682, ρ_1=−0.8,…,0.8); (c) plots of constant ρ_2 for model A (b=0.512, ρ_2 =0.01b,0.5b,0.99b); and (d) plots of constant ρ_2 for model B (b=0.682, ρ_2=0.01b,0.5b,0.99b).

shown to have a second-order wetting transition. The two differ in the local parts, $F[\rho_1(\mathbf{r}),\rho_2(\mathbf{r});b]$, of their free-energy densities, where $\rho_1(\mathbf{r})$ and $\rho_2(\mathbf{r})$ are two densities that define the spatially varying composition of the system. The functions F are a fourth-order polynomial in ρ_1 and ρ_2 for model A, given in Eq. (7), and a sixth-order polynomial for model B, given in Eq. (6).

In the nonwetting regime there is a line tension τ, which is the excess free energy per unit length of the three-phase contact line. It has a finite positive value τ_w at a first-order wetting transition, where it behaves as in Eq. (14) as the wetting transition is approached ($b \to b_w$), but vanishes at a second-order wetting transition as in Eq. (15).

Model B is treated numerically in Sec. III by solving the Euler–Lagrange Eqs. (10) for the interfacial profiles $\rho_1(z)$ and $\rho_2(z)$ far from the contact line and the analogous Eqs. (12) for the full $\rho_1(\mathbf{r})$ and $\rho_2(\mathbf{r})$ in any plane perpendicular to the contact line. The former determine trajectories in the ρ_1,ρ_2 plane that describe the compositions of the interfaces, and are characteristically different for the two models, as seen in Fig. 2(a) for model A and Fig. 2(b) for model B. The exponential decay lengths ξ_1 and ξ_2 with which $\rho_1(z)$ and $\rho_2(z)$ approach their bulk-phase values (8) are given by Eqs. (16) and (17). The interfacial tensions are observed numerically to be given extremely accurately by Eqs. (19) and (20), which are then conjectured to be exact and imply Eq. (21) for b_w. Simple analytical formulas, Eqs. (22) and (23), for the angles in Fig. 2(b), are also found to hold to high numerical accuracy. Formulas (19)–(23) are thus almost surely exact but proving them remains a challenge to analytical theory. That the wetting transition in model B is indeed of second order is seen in Fig. 5, where the numerical results as plotted in Fig. 5(a) are to be compared with the schematic Fig. 1(b).

The line tension in model B is found from the numerically determined $\rho_1(\mathbf{r})$ and $\rho_2(\mathbf{r})$ via the Kerins–Boiteux formula (13) and the results are plotted in Fig. 6. They are seen to satisfy Eq. (4), again consistent with a second-order wetting transition.

Contours of constant $\rho_1(\mathbf{r})$ and $\rho_2(\mathbf{r})$ in any plane perpendicular to the contact line, for models A and B, were determined numerically and are displayed in Fig. 7. They are seen to be characteristically different, those associated with the first-order wetting transition in model A being forklike with inflections, and those for model B being smoother with monotonically varying slopes near the contact line. This distinction between the two models as well as the demonstrated distinction between Eqs. (14) and (15) for the line tension are in accord with earlier results found in interface-displacement models.

ACKNOWLEDGMENTS

We are grateful to Professor J. O. Indekeu for helpful comments and references that have been incorporated in the paper. K.K. acknowledges support by a Grant-in-Aid for Scientific Research and the Next Generation Super Computing Project, Nanoscience Program, Ministry of Education, Culture, Sports, Science and Technology, Japan. B.W. acknowledges support by the National Science Foundation.

[1] J. W. Gibbs, *The Collected Works of J. Willard Gibbs* (Longmans, Green, 1928), Vol. 1, p. 288 (footnote).
[2] J. S. Rowlinson and B. Widom, *Molecular Theory of Capillarity* (Oxford University Press, Oxford, 1982), p. 211.
[3] J. O. Indekeu, K. Ragil, D. Bonn, D. Broseta, and J. Meunier, J. Stat. Phys. **95**, 1009 (1999).
[4] D. Bonn, E. Bertrand, N. Shahidzadeh, K. Ragil, H. T. Dobbs, A. I. Posazhennikova, D. Broseta, J. Meunier, and J. O. Indekeu, J. Phys.: Condens. Matter **13**, 4903 (2001).
[5] S. Dietrich, in *Phase Transitions and Critical Phenomena*, edited by C. Domb and J. L. Lebowitz (Academic, New York 1988), Vol. 12, Chap. 1, pp. 1–218.
[6] A. Oleinikova, I. Brovchenko, and A. Geiger, J. Phys.: Condens. Matter **17**, 7845 (2005).
[7] K. Koga and B. Widom, J. Chem. Phys. **127**, 064704 (2007).
[8] J. Kerins and M. Boiteux, Physica A **117**, 575 (1983).
[9] J. O. Indekeu, Physica A **183**, 439 (1992).
[10] J. O. Indekeu, Int. J. Mod. Phys. B **8**, 309 (1994).
[11] W. H. Press, B. P. Flannery, S. A. Teukolsky, and W. T. Vetterling, *Numerical Recipes in C* (Cambridge University Press, Cambridge, 1998).
[12] J. O. Indekeu, personal communication (30 January 2008).
[13] J. O. Indekeu, Phys. Scr. **T35**, 31 (1991).
[14] J. W. Cahn, J. Chem. Phys. **66**, 3667 (1977).
[15] H. Nakanishi and M. E. Fisher, Phys. Rev. Lett. **49**, 1565 (1982).
[16] H. T. Dobbs and J. O. Indekeu, Physica A **201**, 457 (1993).